

Antiferromagnetic Phase Transition in Four-Layered High- T_c Superconductors $\text{Ba}_2\text{Ca}_3\text{Cu}_4\text{O}_8(\text{F}_y\text{O}_{1-y})_2$ with $T_c = 55\text{--}102\text{ K}$: ^{63}Cu - and ^{19}F -NMR Studies

Sunao SHIMIZU*, Hidekazu MUKUDA, Yoshio KITAOKA, Hijiri KITO¹,
Yasuharu KODAMA¹, Parasharam M. SHIRAGE¹, and Akira IYO¹

Graduate School of Engineering Science, Osaka University, Toyonaka, Osaka 560-8531

¹*National Institute of Advanced Industrial Science and Technology (AIST), Tsukuba, Ibaraki 305-8568*

(Received January 3, 2009; accepted April 6, 2009; published June 10, 2009)

We report on the magnetic characteristics of four-layered high- T_c superconductors $\text{Ba}_2\text{Ca}_3\text{Cu}_4\text{O}_8(\text{F}_y\text{O}_{1-y})_2$ with apical fluorine through ^{63}Cu - and ^{19}F -NMR measurements. The substitution of oxygen for fluorine at the apical site increases carrier density (N_h) and T_c from 55 up to 102 K. The NMR measurements reveal that antiferromagnetic order, which can uniformly coexist with superconductivity, exists up to $N_h \simeq 0.15$, which is somewhat smaller than $N_h \simeq 0.17$, the quantum critical point (QCP) for five-layered compounds. The fact that the QCP for the four-layered compounds moves to a region of lower carrier density than for five-layered ones ensures that a decrease in the number of CuO_2 layers makes an interlayer magnetic coupling weaker.

KEYWORDS: high- T_c superconductivity, copper-oxide, antiferromagnetism, NMR, phase diagram, apical-fluorine
DOI: 10.1143/JPSJ.78.064705

1. Introduction

A markedly high superconducting transition temperature (T_c) in copper oxides has been realized in the multilayered structure of CuO_2 planes. T_c depends on the number of CuO_2 layers (n) in multilayered compounds with a maximum at $n = 3$.¹⁾ In particular, the highest T_c was observed at approximately 133 K in a Hg-based three-layered ($n = 3$) copper oxide $\text{HgBa}_2\text{Ca}_2\text{Cu}_3\text{O}_y$ (Hg-1223).²⁾ Copper oxides with more than three layers comprise inequivalent types of CuO_2 layers: an outer CuO_2 plane (OP) in a five-fold pyramidal coordination and an inner plane (IP) in a four-fold square coordination (see Fig. 1 as example). Site-selective ^{63}Cu -NMR studies have revealed that the local carrier density (N_h) for the IP is smaller than that for the OP. These results in turn revealed a strong relationship between antiferromagnetism (AFM) and superconductivity (SC) inherent to CuO_2 layers into which mobile hole carriers were homogeneously doped.^{3–6)}

The recent systematic Cu-NMR studies of five-layered ($n = 5$) compounds have shown that the AFM order, which can uniformly coexist with SC, is robust up to $N_h \simeq 0.17$, a quantum critical point (QCP) where the AFM order collapses.⁷⁾ This result significantly differs from the well-established results for monolayered ($n = 1$) $\text{La}_{2-x}\text{Sr}_x\text{CuO}_4$ (LSCO)⁸⁾ and bilayered ($n = 2$) $\text{YBa}_2\text{Cu}_3\text{O}_{6+x}$ (YBCO),⁹⁾ in which the AFM order collapses completely by doping an extremely small number of holes of $N_h \sim 0.02$ and 0.055, respectively. These results strongly suggest that the QCP of $n \leq 4$ moves to a region of lower carrier density than that of $n = 5$. Therefore, it is likely that the interlayer magnetic coupling for the onset of the AFM order is enhanced as the number of CuO_2 layers increases. In order to establish how the interlayer magnetic coupling affects the onset of AFM order, we deal with four-layered high- T_c superconductors $\text{Ba}_2\text{Ca}_3\text{Cu}_4\text{O}_8(\text{F}_y\text{O}_{1-y})_2$ with apical fluorine. We note that all these compounds are in an underdoped state of the hole doping regime.

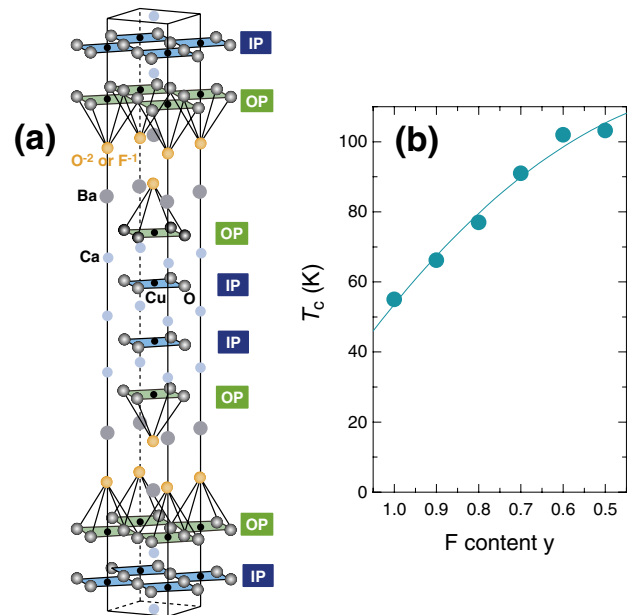


Fig. 1. (Color online) (a) Crystal structure of $\text{Ba}_2\text{Ca}_3\text{Cu}_4\text{O}_8(\text{F}_y\text{O}_{1-y})_2$. This four-layered system includes two crystallographically different CuO_2 planes, namely, IP and OP. (b) T_c vs fluorine content y .¹¹⁾ It shows that the substitution of oxygen for fluorine results in doping hole carriers into CuO_2 layers.

$\text{Ba}_2\text{Ca}_3\text{Cu}_4\text{O}_8(\text{F}_y\text{O}_{1-y})_2$ comprises a stack of four CuO_2 layers as shown in Fig. 1(a). It is known as a new family of multilayered copper oxides with apical fluorine.^{10–13)} The substitution of oxygen (O^{2-}) for apical fluorine (F^{-1}), i.e., a decrease in nominal fluorine content (y), results in the doping of holes into CuO_2 layers, increasing T_c from 55 K at $y = 1.0$ to 102 K at $y = 0.6$, as shown in Fig. 1(b).¹¹⁾ This system provides an opportunity to investigate the characteristics of CuO_2 layers over a wide range of carrier densities, enabling us to focus on the interplay of SC and AFM in an underdoped region.^{14–22)} Here, we may note, in passing, that when $y = 1.0$, the apical fluorine system is a Mott insulator

*E-mail: shimizu@nmr.mp.es.osaka-u.ac.jp

Table I. Lists of T_c and N_h at the OP and IP of $\text{Ba}_2\text{Ca}_3\text{Cu}_4\text{O}_8(\text{F}_y\text{O}_{1-y})_2$. N_h is estimated from the $K_s(T)$ at room temperature (see text). \bar{N}_h is the average carrier density, defined as $[N_h(\text{OP}) + N_h(\text{IP})]/2$. Note that y is the nominal fluorine content.

	$y = 0.6$	$y = 0.7$	$y = 0.8$	$y = 1.0$
T_c	102 K	91 K	77 K	55 K
$N_h(\text{OP})$	+0.207	+0.189	+0.167	+0.148
$N_h(\text{IP})$	+0.165	+0.150	+0.144	(+0.132) ^{a)}
\bar{N}_h	+0.186	+0.170	+0.156	(+0.140) ^{a)}

a) $\bar{N}_h = 0.140$ at $y = 1.0$ is estimated at $N_h(\text{OP}) = 0.148$ on a linear line in the plot of $N_h(\text{OP})$ vs \bar{N}_h (see Fig. 3). A linear extrapolation in the plot in $N_h(\text{IP})$ vs \bar{N}_h gives a tentative $N_h(\text{IP}) = 0.132$ at $\bar{N}_h = 0.140$, since it cannot be estimated directly from the $K_s(T)$ at IP at $y = 1$ (see the open circle in Fig. 3 and the text).

at the nominal composition; however, it exhibits SC. We have discussed in the literature²³⁾ that a possible replacement of O^{-2} for F^{-1} and/or excess oxygen in the BaF layers results in the doping of hole carriers into CuO_2 layers.

In this paper, we report our systematic ^{63}Cu - and ^{19}F -NMR studies of $\text{Ba}_2\text{Ca}_3\text{Cu}_4\text{O}_8(\text{F}_y\text{O}_{1-y})_2$ with $y = 0.6, 0.7, 0.8,$ and 1.0 as the nominal contents. The measurements of ^{63}Cu Knight shift (^{63}K) have revealed that hole carrier density (N_h) increases progressively with decreasing y . The substitution of oxygen for fluorine at the apical site increases N_h and T_c from 55 up to 102 K. The measurements of the ^{63}Cu -NMR spectra and nuclear-spin-lattice-relaxation rate of ^{19}F -NMR [$^{19}(1/T_1)$] show that the AFM order, which can uniformly coexist with SC, exists up to $N_h \simeq 0.15$ being a QCP for the four-layered compounds. From the fact that the QCP of the four-layered compounds moves to a region of lower carrier density than that of the five-layered ones, $N_h \simeq 0.17$, it is ensured that the decrease in the number of CuO_2 layers makes an interlayer magnetic coupling weaker.

2. Experimental

Polycrystalline powder samples of all multilayered systems used in this study were prepared by high-pressure synthesis, as described elsewhere.^{10–12)} Powder X-ray diffraction analysis shows that these compounds almost entirely comprise a single phase, and that the a -axis length continually changes with the nominal fluorine content y .¹¹⁾ T_c was uniquely determined by a sharp onset of diamagnetism using a dc SQUID magnetometer, as summarized in Table I. For NMR measurements, the powder samples were aligned along the c -axis at an external field (H) of ~ 16 T and fixed using stycast 1266 epoxy. The NMR experiments were performed by the conventional spin-echo method in the temperature (T) range of 1.5–300 K with H perpendicular or parallel to the c -axis.

3. Results and Discussion

3.1 Knight shift and local carrier density

Figure 2 indicates typical ^{63}Cu -NMR spectra of the central transition ($1/2 \leftrightarrow -1/2$) for $y =$ (a) 0.6, (b) 0.7, (c) 0.8, and (d) 1.0. The field-swept NMR spectra were measured at H perpendicular to the c -axis. The NMR spectral widths for the samples at room temperature are as narrow as that of Hg-1245,^{5,7)} ensuring the high quality

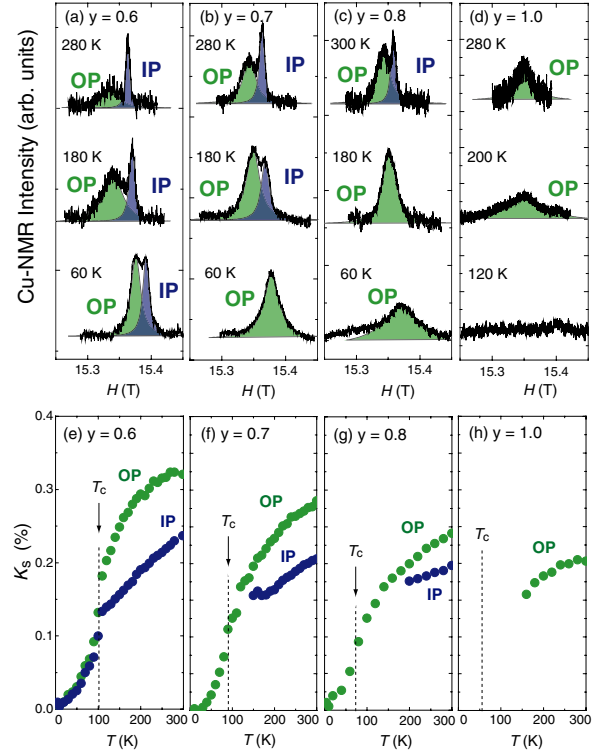


Fig. 2. (Color online) ^{63}Cu -NMR spectra of the central transition ($1/2 \leftrightarrow -1/2$) for $y =$ (a) 0.6, (b) 0.7, (c) 0.8, and (d) 1.0 (cited from ref. 23). The temperature dependence of the Knight shift with H perpendicular to the c -axis for $y =$ (e) 0.6, (f) 0.7, (g) 0.8, and (h) 1.0 (cited from ref. 23).

of the samples. The Cu-NMR spectra of OP and IP are separately detected at $y = 0.6$, whereas the IP's spectra for $y = 0.7$ and 0.8 disappear at low temperatures owing to the development of AFM correlations upon cooling as well as those in the case for the five-layered Hg- or Tl-based compounds.^{5,7)} Interestingly, the NMR spectrum of OP at $y = 1.0$ also disappears at low temperatures, as shown in Fig. 2(d), suggesting the onset of the AFM order at the OP. The systematic variation in the NMR spectra indicates that $\text{Ba}_2\text{Ca}_3\text{Cu}_4\text{O}_8(\text{F}_y\text{O}_{1-y})_2$ becomes underdoped as the nominal fluorine content y increases, which ensures that the substitution of oxygen for the apical fluorine increases N_h .

In general, the Knight shift (K) comprises the T -dependent spin part ($K_s(T)$) and the T -independent orbital part (K_{orb}); $K = K_s(T) + K_{\text{orb}}$. Here, K_{orb} was determined as $0.23 (\pm 0.02)\%$, assuming $K_s \approx 0$ in the $T = 0$ limit. The T dependences of $K_s(T)$ with H perpendicular to the c -axis are displayed in Figs. 2(e)–2(h) for $y = 0.6, 0.7, 0.8,$ and 1.0 , respectively. We evaluated the $K_s(T)$ by fitting the NMR spectra using the Lorentzian function. $K_s(T)$ decreases upon cooling down to T_c for all samples in association with the opening of pseudogap,^{24,25)} whereas its steep decrease below T_c evidences the reduction in spin susceptibility due to the formation of spin-singlet pairing. We note that the empirical relation between $K_s(T)$ at room temperature and the N_h in a CuO_2 plane^{26,27)} allows us to evaluate N_h s at OP and IP for the four samples, which are summarized in Table I along with the T_c and the averaged carrier density \bar{N}_h , defined as $[N_h(\text{OP}) + N_h(\text{IP})]/2$. Figure 3 shows the plot of N_h s at IP and OP against \bar{N}_h . The $N_h(\text{IP})$ at $y = 1.0$, however, was not directly estimated from the $K_s(T)$, because no Cu-NMR

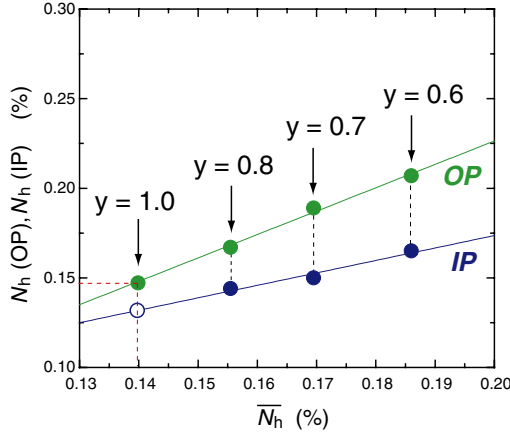


Fig. 3. (Color online) Plots of $N_h(\text{OP})$ and $N_h(\text{IP})$ against average carrier density \bar{N}_h , defined as $[N_h(\text{OP}) + N_h(\text{IP})]/2$. Here, $N_h(\text{OP})$ and $N_h(\text{IP})$ are determined from the Knight shift measurement (see text). $\bar{N}_h = 0.140$ at $y = 1.0$ is estimated from $N_h(\text{OP}) = 0.148$ on a linear line in the plot of $N_h(\text{OP})$ vs \bar{N}_h . A linear extrapolation in the plots of $N_h(\text{IP})$ vs \bar{N}_h gives a tentative $N_h(\text{IP}) = 0.132$ at $\bar{N}_h = 0.140$.

spectrum was detected at room temperature. Instead, $\bar{N}_h = 0.140$ at $y = 1.0$ is estimated from $N_h(\text{OP}) = 0.148$ on a linear line in the plot of $N_h(\text{OP})$ versus \bar{N}_h in Fig. 3. Furthermore, a linear extrapolation in the plot of $N_h(\text{IP})$ vs \bar{N}_h gives a tentative value of $N_h(\text{IP}) = 0.132$ at $\bar{N}_h = 0.140$. As summarized in Table I, the increases of $N_h(\text{OP})$ and $N_h(\text{IP})$ with increasing nominal oxygen content at the apical site increase T_c from 55 to 102 K.

3.2 Zero-field NMR evidence of AFM order

We deal with the AFM order taking place in underdoped CuO_2 layers. The observation of zero-field NMR (ZFNMR) spectra enables us to ensure the onset of the AFM order, since magnetically ordered moments induce the internal magnetic field H_{int} at nuclear sites. Generally, the Hamiltonian for Cu nuclear spin with $I = 3/2$ is described by the Zeeman interaction due to the magnetic field H (\mathcal{H}_Z) and the nuclear-quadrupole interaction (\mathcal{H}_Q) as follows:

$$\begin{aligned} \mathcal{H} &= \mathcal{H}_Z + \mathcal{H}_Q \\ &= -\gamma_N \hbar \mathbf{I} \cdot \mathbf{H} + \frac{e^2 q Q}{4I(2I-1)} [3I_z^2 - I(I+1)], \end{aligned} \quad (1)$$

where γ_N is the Cu nuclear gyromagnetic ratio, eQ is the nuclear quadrupole moment, and eq is the electric field gradient (EFG) at the Cu nuclear site. Here, in \mathcal{H}_Q , the asymmetric parameter (η) is zero in the tetragonal symmetry. Note that the nuclear quadrupole resonance (NQR) frequency $\nu_Q = 3e^2qQ/2\hbar I(2I-1)$. The nuclear Hamiltonian given by eq. (1) is described by H_{int} instead of H for zero-field experiments.

Figure 4(a) shows the Cu-NQR spectrum at $y = 0.6$. The respective ${}^{63}\nu_Q$ s are evaluated as 9.7 and 15 MHz at the IP and OP, which are comparable to ~ 8 –10 and ~ 16 MHz for five-layered systems.^{3–5} Here, the sharp ${}^{63}\text{Cu}$ - and ${}^{65}\text{Cu}$ -NQR spectral widths at ${}^{63}\nu_Q = 22.5$ and ${}^{65}\nu_Q = 20.8$ MHz are as narrow as about 400 kHz. These NQR spectra qualitatively differ from those reported for various copper oxides.^{28–31} The integrated intensities of these NQR spectra are one order of magnitude smaller than those for the

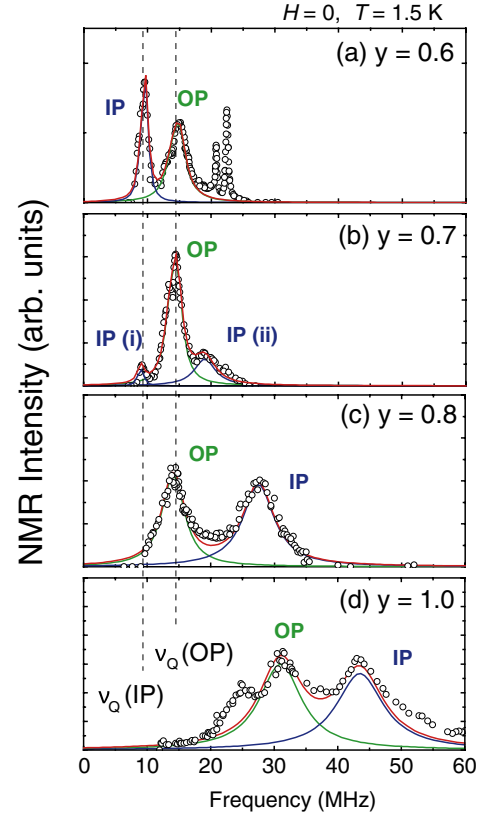


Fig. 4. (Color online) Cu-NQR/ZFNMR spectra at $H = 0$ and $T = 1.5$ K. Green, blue, and red lines represent the spectra for OP, IP, and OP + IP, respectively. All spectra are fitted using the Lorentzian function. As for the asymmetric NQR spectra indicated in (a)–(c), the spectra for the two isotopes of ${}^{63}\text{Cu}$ and ${}^{65}\text{Cu}$ with ${}^{63}Q/{}^{65}Q \sim 1.082$ are superimposed. As for the ZFNMR spectra indicated in (b)–(d) in the AFM ordered state, the spectra for the two isotopes of ${}^{63}\text{Cu}$ and ${}^{65}\text{Cu}$ with a ratio of ${}^{63}\gamma_N/{}^{65}\gamma_N \sim 0.933$ are not clearly resolved because of spectral broadening due to the distribution of H_{int} . (a) The respective Cu-NQR spectra at IP and OP for $y = 0.6$ with ${}^{63}\nu_Q$ s = 9.7 and 15 MHz. Two sharp peaks at 20–25 MHz arise from unknown impurity phases. (b) The Cu-NQR/ZFNMR spectra at $y = 0.7$. The NQR spectrum for the OP is observed with almost the same ${}^{63}\nu_Q$ as that of the OP at $y = 0.6$. The NQR spectrum at IP(i) is observed at 9.1 MHz that is close to ${}^{63}\nu_Q = 9.7$ MHz of the IP at $y = 0.6$, whereas the ZFNMR spectrum at IP(ii) probes the internal field $H_{\text{int}} = 2.4$ T due to the AFM order. The fact that IP(i) and IP(ii) originate from the paramagnetic and AFM phases, respectively, suggests that phase separation takes place because of the closeness of the N_h in the IP to the QCP at which the AFM collapses. (c) Cu-NQR/ZFNMR spectra at $y = 0.8$. The NQR spectrum for the OP is observed at almost the same frequency as that of the OP at $y = 0.6$, revealing that no spontaneous moment is induced at low temperatures. The spectrum observed around 28 MHz arises from the IP with $H_{\text{int}} \sim 2.4$ T and hence the AFM moment $M_{\text{AFM}} \sim 0.12 \mu_B$. (d) The Cu-NMR spectra at $y = 1.0$ with $H_{\text{int}} \sim 2.7$ and 3.8 T for the OP and IP, respectively (cited from ref. 23). Here, $M_{\text{AFM}} = 0.11$ and $0.18 \mu_B$ are estimated for the OP and IP, respectively.

intrinsic phase, which suggests that these NQR spectra arise from some impurity phases containing copper such as starting materials prepared for sample synthesis and intermediate products for high-pressure synthesis.^{10,11,32}

Figure 4(b) shows the Cu-NQR/ZFNMR spectra at $y = 0.7$. The NQR spectrum for OP is observed with almost the same ${}^{63}\nu_Q$ as that of the OP at $y = 0.6$. Note that the respective NQR and ZFNMR spectra at IP(i) and IP(ii) arise from IP. The NQR spectrum at IP(i) is observed at 9.1 MHz that is close to ${}^{63}\nu_Q = 9.7$ MHz of the IP at $y = 0.6$, whereas the ZFNMR spectrum at IP(ii) is observed at ~ 18 MHz.

Assuming that ${}^{63}\nu_Q = 9.1$ MHz and $H_{\text{int}} \perp c$ -axis, $H_{\text{int}} \sim 1.5$ T is estimated for IP(ii). The H_{int} on the CuO_2 plane is generally given by $H_{\text{int}} = |A_{\text{hf}}|M_{\text{AFM}} = |A - 4B|M_{\text{AFM}}$, where A and B are the on-site hyperfine field and super-transferred hyperfine field from the four nearest-neighboring Cu-AFM moments, respectively, and M_{AFM} is the AFM moment.³³ Here, $A \sim 3.7$ T/ μ_B , $B(\text{OP}) \sim 7.4$ T/ μ_B , and $B(\text{IP}) \sim 6.1$ T/ μ_B are assumed to be the same as those for Hg-1245.⁵ Using these values, a uniform AFM moment at IP(ii) is estimated at $M_{\text{AFM}}(\text{IP}) \sim 0.08 \mu_B$ for an AFM phase at $y = 0.7$. The fact that IP(i) and IP(ii) originate from the paramagnetic and AFM phases, respectively, suggests that phase separation takes place because of the closeness of the N_h in the IP to the QCP at which the AFM collapses. The presence of the phase separation probably implies that the AFM critical point could be close to $N_h \sim 0.15$.

Figure 4(c) indicates the Cu-NQR/ZFNMR spectra at $y = 0.8$. The spectrum observed around 14.4 MHz arises from the OP since its peak frequency is almost the same as ${}^{63}\nu_Q = 15$ MHz for the OP at $y = 0.6$. Accordingly, another spectrum around 28 MHz is assigned to arise from IP. Using the above-mentioned parameters, $H_{\text{int}} \sim 2.4$ T and $M_{\text{AFM}}(\text{IP}) \sim 0.12 \mu_B$ are estimated for the IP at $y = 0.8$.

Figure 4(d) shows the Cu-ZFNMR spectra observed around 30 and 45 MHz at $H = 0$ for $y = 1.0$. When noting that ZFNMR spectra are absent around ${}^{63}\nu_Q(\text{IP}) = 8$ –10 MHz and ${}^{63}\nu_Q(\text{OP}) = 14$ –16 MHz, the observation of the NMR spectra around 30 and 45 MHz demonstrates that H_{int} s are present at the respective IP and OP with $H_{\text{int}} \sim 3.8$ and 2.7 T. Since $N_h(\text{OP}) > N_h(\text{IP})$ due to the charge imbalance between the OP and the IP and hence $M_{\text{AFM}}(\text{OP}) < M_{\text{AFM}}(\text{IP})$, $M_{\text{AFM}}(\text{OP}) \sim 0.11$ and $M_{\text{AFM}}(\text{IP}) \sim 0.18 \mu_B$ are evaluated at the OP and IP, respectively, using the relation $H_{\text{int}} = |A_{\text{hf}}|M_{\text{AFM}} = |A - 4B|M_{\text{AFM}}$. Notably, the OP, which is mainly responsible for the SC with $T_c = 55$ K, manifests the AFM order, leading us to the conclusion that the uniform mixing of AFM with $M_{\text{AFM}} = 0.11 \mu_B$ and SC at $T_c = 55$ K occurs in the OP as well as in the three IPs of the five-layered systems.⁷

3.3 ${}^{19}\text{F}$ -NMR probe of Néel temperature

Here, we would like to discuss the results from ${}^{19}\text{F}$ -NMR measurements. Figure 5 shows ${}^{19}\text{F}$ -NMR spectra at $T = 300$ K. The Knight shift at $H \parallel c$ -axis, ${}^{19}K_c$, is slightly different from that at $H \perp c$ -axis, ${}^{19}K_{ab}$. The ${}^{19}K_c$ is estimated to be $\sim 0.15\%$, and decreases with increasing y , indicating that the local environments at fluorine gradually change with hole-doping level. In addition to that, the NMR spectra for (d) $y = 1.0$ are somewhat broader than the others probably owing to the inclusion of some impurity phase related to off-stoichiometry.

The Néel temperatures (T_N s) at $y = 0.7, 0.8$, and 1.0 are determined by ${}^{19}\text{F}$ - T_1 measurement, which sensitively probes critical magnetic fluctuations developing at the OP and the IP as the system approaches an AFM order. Generally, $1/T_1$ is described as

$$\frac{1}{T_1} = \frac{2\gamma_N^2 k_B T}{(\gamma_c \hbar)^2} \sum_{\mathbf{q}} |A_{\mathbf{q}}|^2 \frac{\text{Im}[\chi(\mathbf{q}, \omega_0)]}{\omega_0}, \quad (2)$$

where $A_{\mathbf{q}}$ is the wave-vector (\mathbf{q})-dependent hyperfine-coupling constant, $\chi(\mathbf{q}, \omega)$ is the dynamical spin suscepti-

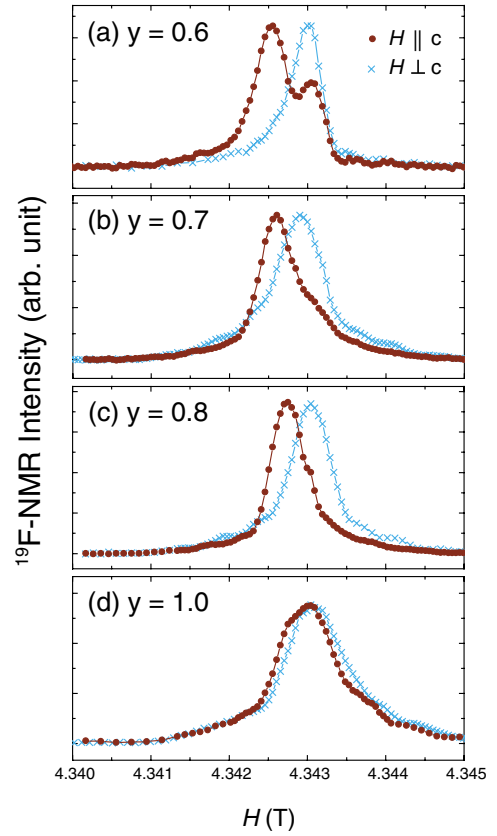


Fig. 5. (Color online) ${}^{19}\text{F}$ -NMR spectra measured at $T = 300$ K for $y =$ (a) 0.6, (b) 0.7, (c) 0.8, and (d) 1.0 at $\omega_0 = 174.2$ MHz. The direction of H is parallel to the c -axis (solid circle) and perpendicular to the c -axis (cross). The NMR spectra for (d) $y = 1.0$ are somewhat broader than the others, which is probably due to the inclusion of some impurity phases related to off-stoichiometry.

bility, and ω_0 is the NMR frequency. The T dependence of $1/T_1$ shows a peak at T_N because the low-energy spectral weight in $\chi(\mathbf{q} = \mathbf{Q}, \omega)$ is strongly enhanced around $\omega_0 \sim 0$ in association with the divergence of magnetic correlation length at $T \sim T_N$. Here, \mathbf{Q} is the AFM wave vector ($\pi/a, \pi/a$). ${}^{19}(1/T_1)$ at $H \parallel c$ -axis is presented for all samples in Fig. 6. In the present case, the relaxation processes in $1/T_1$ compose of quasiparticle contributions probing the onset of SC and the magnetic one probing magnetic fluctuations. However, we consider that the former is negligible in the case of $1/T_1$ at the apical site; in fact, it has been reported that $1/T_1$ at the apical oxygen by ${}^{17}\text{O}$ -NMR did not change markedly at T_c ³⁴ because of the very small hyperfine-coupling constant with the quasiparticles in CuO_2 layers. In this context, ${}^{19}(1/T_1)$ is expected to be dominated by magnetic fluctuations.

The respective Figs. 6(b) and 6(c) show the T dependences of ${}^{19}(1/T_1)$ s at $y = 0.7$ and 0.8, exhibiting peaks at ~ 30 and 50 K. This result ensures the AFM order at $T_N = 30$ and 50 K for IP(ii) at $y = 0.7$ and IP at $y = 0.8$ with a spontaneous AFM moment of $M_{\text{AFM}}(\text{IP(ii)}) \sim 0.08 \mu_B$ and $M_{\text{AFM}}(\text{IP}) \sim 0.12 \mu_B$, respectively. Note that the absence of a peak in $1/T_1$ at $y = 0.6$ evidences that this compound is in the paramagnetic state down to 4.2 K. As shown in Fig. 6(d) for $y = 1.0$, there are a distinct peak in $1/T_1$ at $T_N \sim 80$ K and a significant peak at $T_N^* \sim 30$ K. The AFM order inherent to the OP responsible for SC is presumably

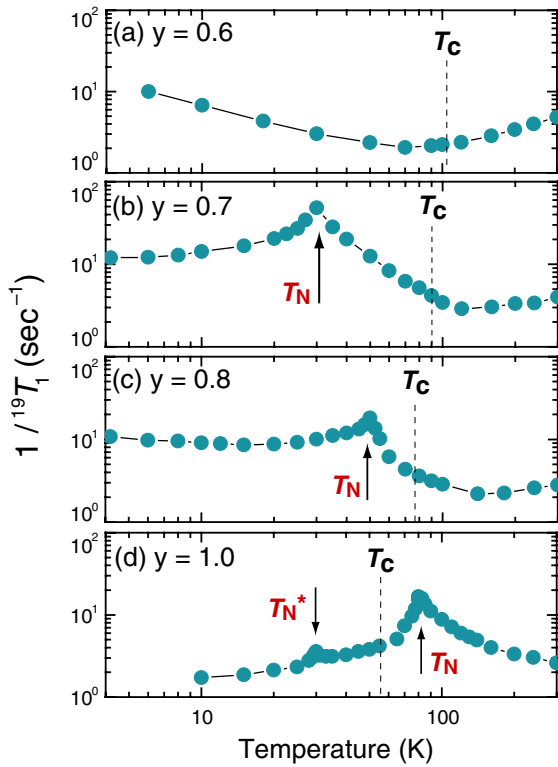


Fig. 6. (Color online) The temperature dependences of $^{19}T_1$ s for $y =$ (a) 0.6, (b) 0.7, (c) 0.8, and (d) 1.0 (cited from ref. 23) at $\omega_0 = 174.2$ MHz and $H \parallel c$ -axis. For (a) $y = 0.6$, the reason for $1/T_1$ increasing upon cooling is associated with the development of magnetic correlations at low temperatures. For $y =$ (b) 0.7 and (c) 0.8, $1/T_1$ exhibits a peak at $T_N \sim 30$ and 50 K, respectively. (d) There are a distinct peak in $1/T_1$ at $T_N \sim 80$ K and a significant peak at $T_N^* \sim 30$ K. The AFM order inherent to the OP responsible for SC is presumably developed below T_N^* , exhibiting the spontaneous AFM moment of $M_{AFM}(OP) \sim 0.11 \mu_B$ at low temperatures.

developed below $T_N^* \sim 30$ K, exhibiting the spontaneous AFM moment of $M_{AFM}(OP) \sim 0.11 \mu_B$ at low temperatures. This suggests that the SC uniformly coexists with the AFM order in a single CuO_2 plane with $N_h \sim 0.148$. Since $N_h(IP) < N_h(OP)$ and $M_{AFM}(IP) > M_{AFM}(OP)$, the T_N at the IP becomes larger than at the OP. It is noteworthy that $T_N^* \sim 30$ K for the OP at $y = 1.0$ is comparable to the $T_N \sim 30$ K for IP(ii) at $y = 0.7$ because both layers possess almost the same N_h .

3.4 Phase diagram of AFM and SC

Figure 7 shows the phase diagram of AFM and SC as a function of N_h where T_c and $T_N(T_N^*)$ are plotted against N_h for the OPs and IPs of the four-layered superconductors $\text{Ba}_2\text{Ca}_3\text{Cu}_4\text{O}_8(\text{F}_y\text{O}_{1-y})$ at $y = 0.6, 0.7, 0.8,$ and 1.0 . We note that a uniform mixing of AFM ($T_N = 30$ K) and SC ($T_c = 55$ K) was observed for the OP at $y = 1.0$, which strongly suggests that it is a general property inherent to a single CuO_2 plane in the underdoped regime for hole doping. It has been reported in the literature^{4,7} that the bulk T_c of multilayered compounds was determined by the T_c of the OP and that the T_c of the IP was significantly lower than the bulk T_c owing to the lower N_h at the IP. In the phase diagram in Fig. 7, the QCP in the four-layered system is obtained at $N_h \simeq 0.15$ smaller than $N_h \simeq 0.17$ for the five-layered system,⁷ suggesting that the interlayer magnetic coupling of

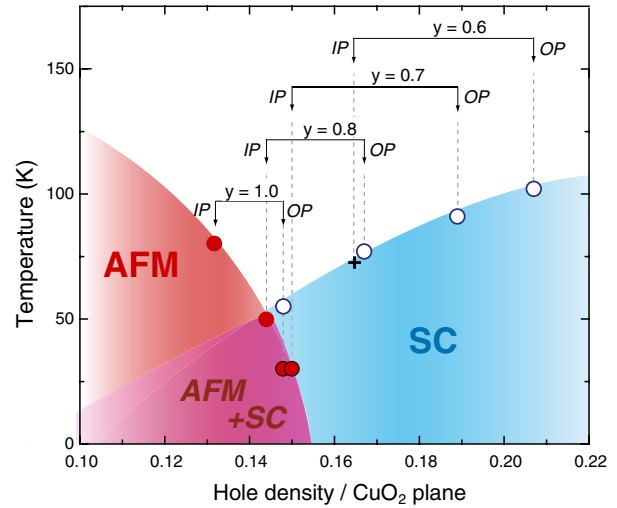


Fig. 7. (Color online) Phase diagram of AFM and SC as a function of hole carrier density N_h . T_c (indicated by open circle) and T_N (closed circle) are plotted against N_h for the OPs and IPs of $\text{Ba}_2\text{Ca}_3\text{Cu}_4\text{O}_8(\text{F}_y\text{O}_{1-y})$ at $y = 0.6, 0.7, 0.8,$ and 1.0 . N_h was determined from the Knight shift measurement (see the text). The $T_c \sim 70$ K for the IP at $y = 0.6$, which is shown by black plus (+) was determined from a small peak at $T \sim 70$ K in the T derivative of the Knight shift (dK/dT) as well as in the literature.^{3,7} Note that the uniform mixing of AFM ($T_N = 30$ K) and SC ($T_c = 55$ K) takes place at the OP at $y = 1.0$. This result strongly suggests that it is a general property inherent to a single CuO_2 plane in the underdoped regime for hole doping.^{6,7}

the four-layered compound is smaller than that of the five-layered compound. The phase diagrams of AFM and SC in multilayered systems are markedly different from the well-established ones in LSCO ($n = 1$)⁸ and YBCO ($n = 2$),⁹ where the AFM order totally collapses by doping a very small number of holes with $N_h \sim 0.02$ and 0.055 , respectively. The reason why the AFM phase exists up to $N_h \simeq 0.15$ and 0.17 in the four- and five-layered compounds, respectively, is that the interlayer magnetic couplings are stronger than in LSCO or YBCO owing to the existence of homogeneously underdoped IPs.

4. Conclusions

The extensive Cu-NMR/NQR and F-NMR measurements on the four-layered high- T_c superconductors $\text{Ba}_2\text{Ca}_3\text{Cu}_4\text{O}_8(\text{F}_y\text{O}_{1-y})$ have unraveled the systematic evolution of AFM and SC as the function of hole carrier density N_h ; T_c and T_N are controlled by the substitution of oxygen for fluorine at the apical site. It is demonstrated that the AFM order, which can uniformly coexist with SC, exists up to $N_h \simeq 0.15$, reinforcing that the uniform mixing of AFM and SC is a general property inherent to a single CuO_2 plane in the underdoped regime for hole doping. $N_h \simeq 0.15$ at QCP for the four-layered compounds is somewhat smaller than $N_h \simeq 0.17$ for the five-layered compounds. The fact that the QCP for the four-layered compounds moves to a region of lower carrier density than for the five-layered compounds ensures that the decrease in the number of CuO_2 layers makes interlayer magnetic coupling weaker. The present studies have highlighted the intimate evolution of AFM and SC in the phase diagram inherent to the homogeneously doped CuO_2 plane, which depends on the interlayer magnetic coupling significantly.

Acknowledgments

The authors are grateful to M. Mori, T. Tohyama, H. Eisaki, and M. Ogata for their helpful discussions. This work was supported by a Grant-in-Aid for Specially Promoted Research (20001004) and in part by Global COE Program (Core Research and Engineering of Advanced Materials Science), from the Ministry of Education, Culture, Sports, Science and Technology (MEXT), Japan. One of the authors (S.S.) is financially supported as a JSPS (the Japan Society for the Promotion of Science) Research Fellow.

- 1) B. A. Scott, E. Y. Suard, C. C. Tsuei, D. B. Mitzi, T. R. McGuire, B.-H. Chen, and D. Walker: *Physica C* **230** (1994) 239.
- 2) A. Schilling, M. Cantoni, J. D. Guo, and H. R. Ott: *Nature (London)* **363** (1993) 56.
- 3) Y. Tokunaga, K. Ishida, Y. Kitaoka, K. Asayama, K. Tokiwa, A. Iyo, and H. Ihara: *Phys. Rev. B* **61** (2000) 9707.
- 4) H. Kotegawa, Y. Tokunaga, K. Ishida, G.-q. Zheng, Y. Kitaoka, H. Kito, A. Iyo, K. Tokiwa, T. Watanabe, and H. Ihara: *Phys. Rev. B* **64** (2001) 064515.
- 5) H. Kotegawa, Y. Tokunaga, Y. Araki, G.-q. Zheng, Y. Kitaoka, K. Tokiwa, K. Ito, T. Watanabe, and A. Iyo: *Phys. Rev. B* **69** (2004) 014501.
- 6) H. Mukuda, M. Abe, Y. Araki, Y. Kitaoka, K. Tokiwa, T. Watanabe, A. Iyo, H. Kito, and Y. Tanaka: *Phys. Rev. Lett.* **96** (2006) 087001.
- 7) H. Mukuda, Y. Yamaguchi, S. Shimizu, Y. Kitaoka, P. Shirage, and A. Iyo: *J. Phys. Soc. Jpn.* **77** (2008) 124706.
- 8) B. Keimer, N. Belk, R. J. Birgeneau, A. Cassanho, C. Y. Chen, M. Greven, and M. A. Kastner: *Phys. Rev. B* **46** (1992) 14034.
- 9) S. Sanna, G. Allodi, G. Concas, A. D. Hillier, and R. De Renzi: *Phys. Rev. Lett.* **93** (2004) 207001.
- 10) A. Iyo, Y. Tanaka, M. Tokumoto, and H. Ihara: *Physica C* **366** (2001) 43.
- 11) A. Iyo, M. Hirai, K. Tokiwa, T. Watanabe, and Y. Tanaka: *Physica C* **392–396** (2003) 140.
- 12) A. Iyo, Y. Tanaka, H. Kito, Y. Kodama, P. M. Shirage, D. D. Shivagen, H. Matsuhata, K. Tokiwa, and T. Watanabe: *J. Phys. Soc. Jpn.* **76** (2007) 094711.
- 13) P. M. Shirage, D. D. Shivagan, Y. Tanaka, Y. Kodama, H. Kito, and A. Iyo: *Appl. Phys. Lett.* **92** (2008) 222501.
- 14) M. Inaba, H. Matsukawa, M. Saitoh, and H. Fukuyama: *Physica C* **257** (1996) 299.
- 15) S. C. Zhang: *Science* **275** (1997) 1089.
- 16) A. Himeda and M. Ogata: *Phys. Rev. B* **60** (1999) R9935.
- 17) Y. S. Lee, R. J. Birgeneau, M. A. Kastner, Y. Endoh, S. Wakimoto, K. Yamada, R. W. Erwin, S.-H. Lee, and G. Shirane: *Phys. Rev. B* **60** (1999) 3643.
- 18) Y. Sidis, C. Ulrich, P. Bourges, C. Bernhard, C. Niedermayer, L. P. Regnault, N. H. Andersen, and B. Keimer: *Phys. Rev. Lett.* **86** (2001) 4100.
- 19) R. I. Miller, R. F. Kiefl, J. H. Brewer, J. E. Sonier, J. Chakhalian, S. Dunsiger, G. D. Morris, A. N. Price, D. A. Bonn, W. H. Hardy, and R. Liang: *Phys. Rev. Lett.* **88** (2002) 137002.
- 20) B. Lake, H. M. Ronnow, N. B. Christensen, G. Aeppli, K. Lefmann, D. F. McMorrow, P. Vorderwisch, P. Smeibidl, N. Mangkorntong, T. Sasagawa, M. Nohara, H. Takagi, and T. E. Mason: *Nature (London)* **415** (2002) 299.
- 21) T. K. Lee, C.-M. Ho, and N. Nagaosa: *Phys. Rev. Lett.* **90** (2003) 067001.
- 22) E. Demler, W. Hanke, and S. C. Zhang: *Rev. Mod. Phys.* **76** (2004) 909.
- 23) S. Shimizu, T. Sakaguchi, H. Mukuda, Y. Kitaoka, P. M. Shirage, Y. Kodama, and A. Iyo: *Phys. Rev. B* **79** (2009) 064505.
- 24) H. Yasuoka, T. Imai, and T. Shimizu: in *Strong Correlation and Superconductivity*, ed. H. Fukuyama, S. Maekawa, and A. P. Malozemoff (Springer, Berlin, 1989) Vol. 89, p. 254.
- 25) R. E. Walstedt: *The NMR Probe of High- T_c Materials* (Springer, Berlin, 2008).
- 26) G.-q. Zheng, Y. Kitaoka, K. Ishida, and K. Asayama: *J. Phys. Soc. Jpn.* **64** (1995) 2524.
- 27) Y. Tokunaga, H. Kotegawa, K. Ishida, G.-q. Zheng, Y. Kitaoka, K. Tokiwa, A. Iyo, and H. Ihara: *J. Low Temp. Phys.* **117** (1999) 473.
- 28) K. Ishida, Y. Kitaoka, N. Ogata, T. Kamino, K. Asayama, and J. R. Cooper: *J. Phys. Soc. Jpn.* **62** (1993) 2803.
- 29) S. Ohsugi, Y. Kitaoka, K. Ishida, G.-q. Zheng, and K. Asayama: *J. Phys. Soc. Jpn.* **63** (1994) 700.
- 30) S. Ohsugi, T. Tsuchiya, T. Koyama, and K. Fueki: *J. Low Temp. Phys.* **105** (1996) 419.
- 31) G.-q. Zheng, Y. Kitaoka, K. Asayama, K. Hamada, H. Yamauchi, and S. Tanaka: *Physica C* **260** (1996) 197.
- 32) N. Kobayashi, Z. Hiroi, and M. Takano: *J. Solid State Chem.* **132** (1997) 274.
- 33) F. Mila and T. M. Rice: *Phys. Rev. B* **40** (1989) 11382.
- 34) P. C. Hammel, M. Takigawa, R. H. Heffner, Z. Fisk, and C. Ott: *Phys. Rev. Lett.* **63** (1989) 1992.